

Article

MOF-801/Graphene Adsorbent Material for Greenhouse Climate Control System—Numerical Investigation

Andrew N. Aziz ^{1,2,*} , Raya Al-Dadah ¹, Saad Mahmoud ¹, Mohamed A. Ismail ^{3,4}, Mohammed K. Almesfer ³, Marwa F. El-Kady ⁵  and Hassan Shokry ⁶ 

- ¹ Department of Mechanical Engineering, University of Birmingham, Edgbaston, Birmingham B15 2TT, UK
² City of Scientific Research and Technological Applications, SRTA-City, New Borg El Arab City 21934, Egypt
³ Department of Chemical Engineering, College of Engineering, King Khalid University, Abha 61411, Saudi Arabia
⁴ Institute of Engineering Research and Materials Technology, National Center for Research, Khartoum 2424, Sudan
⁵ Chemical and Petrochemical Engineering Department, Egypt-Japan University of Science and Technology (E-JUST), New Borg El-Arab City 21934, Egypt
⁶ Environmental Engineering Department, Egypt-Japan University of Science and Technology (E-JUST), New Borg El-Arab City 21934, Egypt
* Correspondence: andrewnabil.dr18@gmail.com

Abstract: Greenhouses with efficient controlled environment offer a promising solution for food security against the impacts of increasing global temperatures and growing water scarcity. However, current technologies used to achieve this controlled environment consume a significant amount of energy, which impacts on operational costs and CO₂ emissions. Using advanced metal organic framework materials (MOFs) with superior water adsorption characteristics, this work investigates the development of a new technology for a greenhouse-controlled environment. The system consists of MOF coated heat exchanger, air to air heat exchanger, and evaporative cooler. A three-dimensional computational fluid dynamics (CFD) model was developed using COMSOL software and experimentally validated for the MOF-801/Graphene coated heat exchanger (DCHE) to determine the best cycle time and power input. It was found that using desorption time of 16 min and power input of 1.26 W, the maximum water removal rate was obtained from MOF-801/Graphene of 274.4 g/kg_{MOF}/W.hr. In addition, an overall mathematical model for the greenhouse climate control was developed and used to investigate the effects of air humidity and velocity on the input air conditions to the greenhouse. Results showed that with high relative humidity levels of 90% in the greenhouse can be conditioned to reach the required relative humidity of 50%.

Keywords: modelling; simulation; MATLAB; COMSOL; MOF-801/Graphene; adsorption



Citation: Aziz, A.N.; Al-Dadah, R.; Mahmoud, S.; Ismail, M.A.; Almesfer, M.K.; El-Kady, M.F.; Shokry, H. MOF-801/Graphene Adsorbent Material for Greenhouse Climate Control System—Numerical Investigation. *Energies* **2023**, *16*, 3864. <https://doi.org/10.3390/en16093864>

Academic Editor: Konstantinos Christoforidis

Received: 20 March 2023

Revised: 26 April 2023

Accepted: 28 April 2023

Published: 1 May 2023



Copyright: © 2023 by the authors. Licensee MDPI, Basel, Switzerland. This article is an open access article distributed under the terms and conditions of the Creative Commons Attribution (CC BY) license (<https://creativecommons.org/licenses/by/4.0/>).

1. Introduction

The rapid world population growth, projected to reach 9.8 billion by 2050, combined with adverse climate changes are making food security a global challenge [1]. Food security depends on adequate crop production which is adversely affected by the extreme temperatures in hot climates, lack of irrigation water, and poor soil quality [2]. Controlled environment agriculture (CEA) in greenhouses offers a promising solution to boost food security against the impacts of increasing global temperatures and growing water scarcity [3]. The main challenge is to provide a suitable greenhouse indoor environment where the required temperature and humidity distribution are maintained with low cost and low environmental impacts [4]. A high level of relative humidity occurring inside greenhouses, especially during the night period, increases the risk of condensation on the leaves, leading to botrytis, fungal, and bacterial diseases. Moreover, lower relative humidity rate inhibits the crop growth, induces water stress in the crops, and reduces the stem length

and leaf sizes [5]. As for the greenhouse temperature, overheating is a serious problem for plant growth and production, particularly in arid and semi-arid regions with high solar radiation [3].

Various types of greenhouse cooling technologies have been proposed for greenhouse climate control [3,4]. Passive cooling methods, e.g., natural ventilation and shading nets, are simple and low-cost technologies for reducing greenhouse temperatures, however, their efficiency is limited [6,7]. Therefore, active cooling methods, such as evaporative pads, fogging, misting, and fan ventilation, are used in warm climates. Despite their higher cooling efficiency, however, they require significant amounts of energy and water [8,9]. Therefore, there is a need for an active cooling technology with low energy consumption capable of achieving the target temperature and humidity conditions.

Desiccant cooling systems are effective in hot and arid regions, as they are based on the combination of the cooling and the dehumidification of the ambient air by using either solid or liquid desiccant materials. They can operate using low grade waste heat or renewable thermal energy sources and produce higher air quality. In addition, they enable zero ozone depletion and global warming potential due to using no refrigerants. Liquid desiccant cooling systems for greenhouse climate control have been proposed by many researchers [10,11], while some researchers investigated the use of solid desiccants [12,13]. A drawback associated with liquid desiccants is that they are capable of chemically reacting with moist air and show possibilities of harming people who would breathe the air. On the other hand, solid desiccants are highly durable, environmentally friendly, and inexpensive when compared to liquid desiccants [14]. Moreover, solid desiccant systems are compact and can be integrated easily into the existing greenhouse air conditioning systems, unlike liquid desiccant systems that require tower beds and additional fan power [15].

Desiccant-coated heat exchangers (DCHXs) have been investigated recently by many researchers as a new system for climate control in various applications. Saeed and Al-Alili [16] reviewed the experimental and modelling studies of DCHXs and concluded that SAPO34 outperforms silica gel and FAPO 34 in terms of moisture removal rate. Vivekh et al. [14] reviewed the developments in DCHXs and showed that the composite LiCl/silica gel desiccants performed better than pure counterparts. Ge et al. [17,18] and Hu et al. [19] studied different silica gel composites, including silica gel/potassium formate, silica gel/sodium acetate, and silica gel/lithium chloride, for composite desiccant coated heat exchangers and found that their dehumidification capacity improved significantly compared to pure silica gel DCHX. Therefore, most of the reported studies on DCHXs have investigated conventional adsorbent materials like silica gel, zeolites and composite of silica with hygroscopic salts. In addition, it was recommended that new desiccants with higher sorption uptake capacity, S-shape isotherms, and faster kinetics be developed to ensure that regeneration can occur at lower temperatures [14].

Metal-organic frameworks (MOFs) are porous crystalline materials constructed from metal ions connected in three-dimensional structure by organic ligands. They have attracted significant interest due to their high porosity, structural versatility, and high stability. MOFs have been widely investigated for water sorption-based applications [20], including seawater desalination [21], cooling [22], energy storage, humidity control in buildings, and water harvesting from air. Hussein et al. [23] studied various MOF materials like MIL-101(Cr), CPO-27(Ni), MIL-100(Fe), and Aluminium fumarate and their composites, showing their high water adsorption capability and potential for heat pump applications. Kapteijn et al. [24] reported that aluminium fumarate MOF material has higher water uptake compared with SAPO-34 and thus can be used for humidity control applications. Recently, Yaghi and co-workers reported the development of MOF-801 and MOF-303 for atmospheric water harvesting, showing their ability to be regenerated at low heating temperature (<90 °C) and high-water uptake at low RH (<0.2). Zirconium-based MOFs like MOF-801 represent some of the most investigated MOFs due to their exceptional stability and topological diversity [25]. Solovyeva et al. [26] studied the dynamics and equilibrium of MOF-801/water adsorption and showed that the efficiency

and the power of the adsorption cooling cycle, achievable with the “MOF-801/water” working pair, are attractive for adsorption cooling. However, the thermal conductivity of these MOFs are low due to the short phonon path and the low atomic density, which adversely affects their performance in adsorption systems. Diab et al. [27] reviewed various methods for enhancing the thermal conductivity of MOFs and concluded that adding graphene nanoplatelets to the neat MOF-801 resulted a significant increase of its thermal conductivity. In this work, MOF-801/Graphene was used to develop a wire finned coated heat exchanger for climate control of a greenhouse to achieve the required humidity and temperature levels.

2. MOF-801/Graphene Synthesis and Characterization

MOF-801/Graphene was synthesized according to the process described by Diab et al. [27], whereby a mixture of $ZrCl_4$ (1.16 g) and fumaric acid (0.55 g) was completely dissolved in DMF (150 mL) dispersed with 0.1 g of graphene nanoplatelets. Then, 10.5 mL acetic acid and 0.460 mL Triethylamine were added. The solution was transferred into a 100 mL capped bottle and kept in an oven overnight at temperature of 100 °C. The resulting solution was allowed to cool down, and the precipitate was isolated by centrifugation and washed with Methanol. Subsequently, the precipitate was immersed in Methanol (80 mL) for 36 h, during which Methanol was refreshed every 12 h. Finally, the grey powder was collected by centrifugation and dried in an oven for 24 h.

Diab et al. investigated MOF-801 with 10%, 20%, and 30% wt.% of graphene nanoplatelets and concluded that 10% graphene is the most appropriate ratio since increasing the graphene percentage by more than 10% will decrease the surface area to half (420 m²/g in the case of 20% graphene). Therefore, MOF-801/10 wt.% graphene nanoplates composite is used in this work.

The highly dispersed MOF-801 nanoparticles on graphene nanoplatelets were visualized using high-resolution transmission electron microscopy (HRTEM). Figure 1 shows the TEM images, highlighting that the MOF particles are synthesized in nanoscale sizes to suitably graze the nanoparticles on graphene nanoplatelets ranging from 350 nm to 5 nm. Graphene nanoplatelets serve as nucleating surfaces for forming MOF-801 nanoparticles, resulting in a homogeneous and well-coated MOF layer on graphene sheets. Figure 2a shows the PXRD pattern for MOF-801 nanoparticles, graphene nanoplatelets, and MOF-801/Graphene composite measured using a D8 Bruker X-ray powder diffractometer at room temperature [27].

Thermal stability is important in the development of MOF materials where thermogravimetric analysis (TGA) and high temperature XRD measurements are used [28]. To assess the thermal stability of MOF-801 and MOF-801/Graphene nanoplatelets, a TGA/DCS system was used where samples were heated from 25 to 700 °C at a rate of 10 °C/min under a constant flow of air. Figure 2b shows the TGA results, highlighting that MOF-801/Graphene nanoplatelets have higher thermal stability than MOF-801, suggesting that the developed composite is thermally stable and can be utilized at relatively high temperatures [27].

Figure 3 represents the measured water adsorption isotherm of MOF-801/Graphene at 25 °C, 45 °C, and 55 °C. It is clear that the MOF-801/Graphene exhibited a type I adsorption isotherm, reaching 71.5% of its maximum capacity at a low relative pressure of 0.2, with a final uptake of 0.35 g HO₂ gads⁻¹ at a relative pressure of 0.9.

Figure 4 shows eight cycles for the adsorption/desorption of MF-801/Graphene, indicating good stability, and a desorption temperature of 90 °C is enough to produce a repeatable desorption process. The addition of graphene nanoplatelets reduced the cyclic time compared to the neat MOF-801.

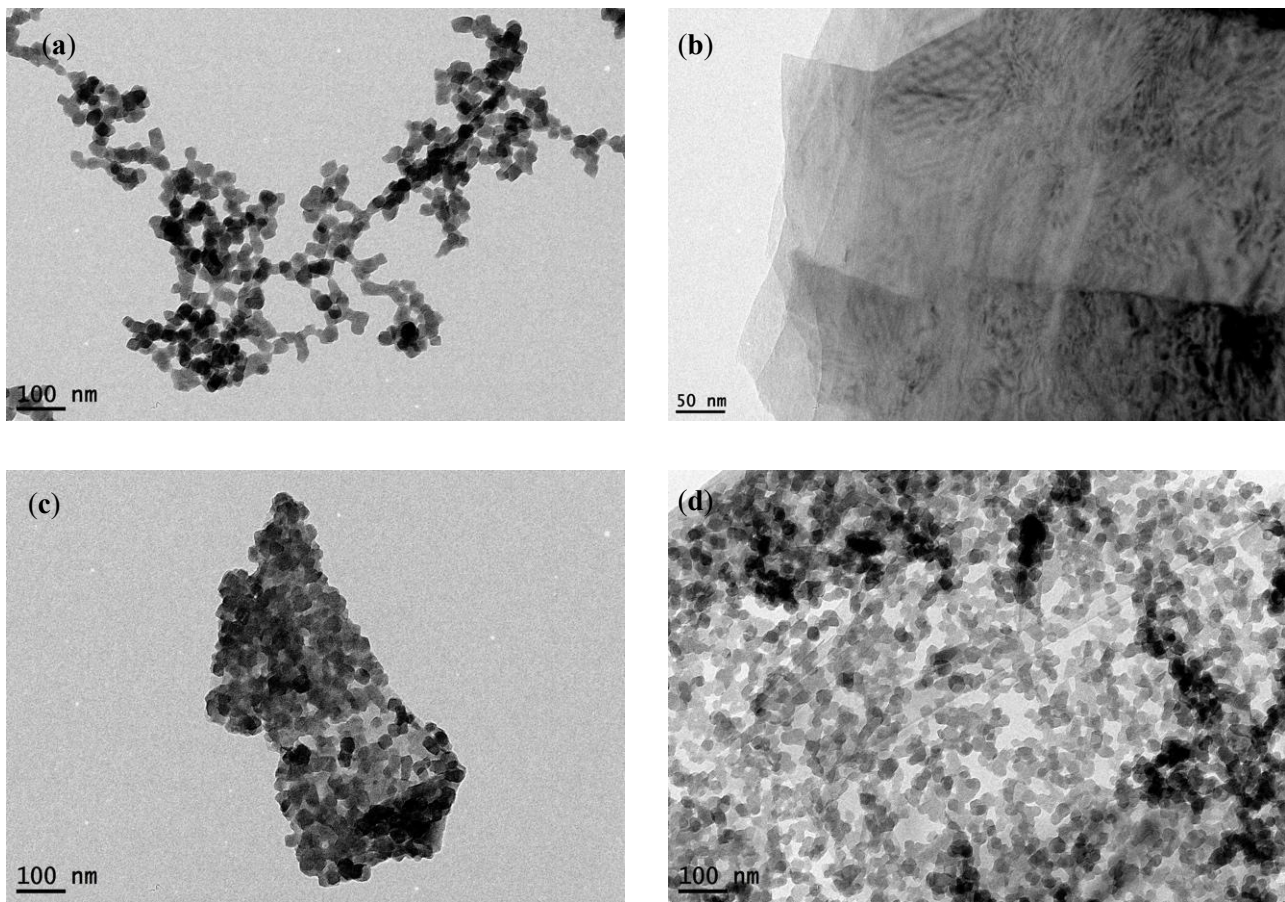


Figure 1. (a) TEM image of MOF-801 nanoparticles. (b) TEM image of graphene nanoplatelets. (c,d) TEM images of MOF-801/Graphene [27].

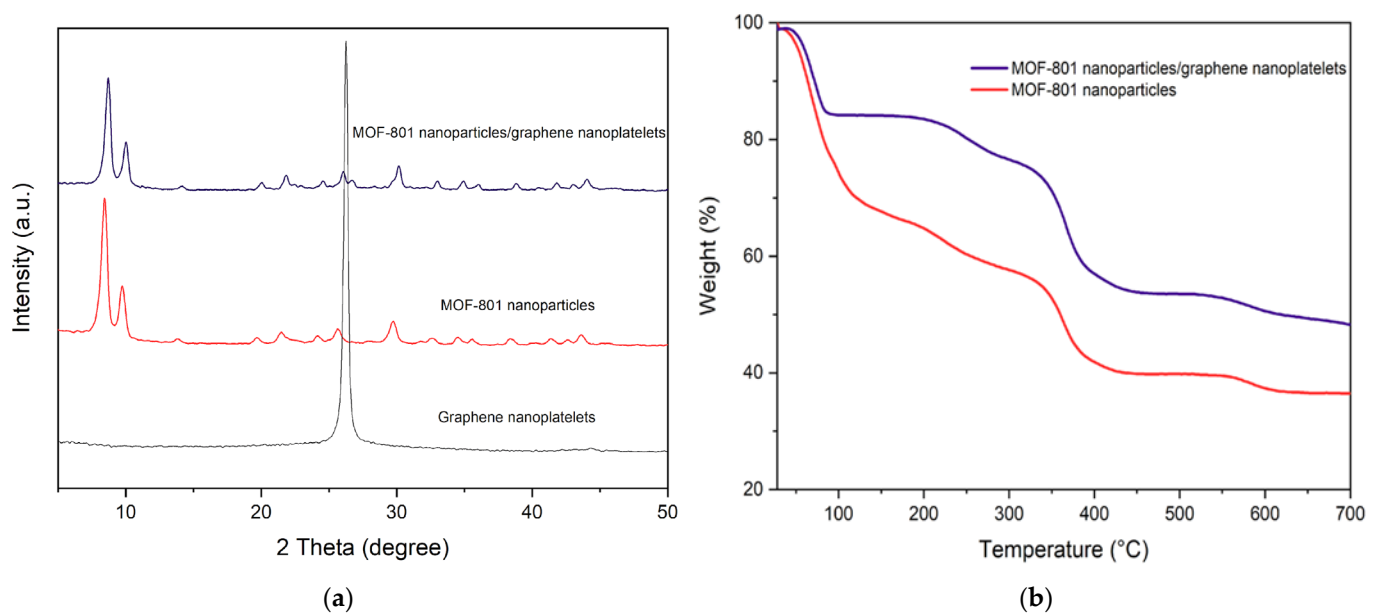


Figure 2. (a) PXRDs patterns for graphene nanoplatelets, neat MOF-801 nanoparticles, and MOF-801 nanoparticles/Graphene nanoplatelets (10%) composite [27]; (b) TGAs for neat MOF-801 nanoparticles, and MOF-801 nanoparticles/graphene nanoplatelets composite [27].

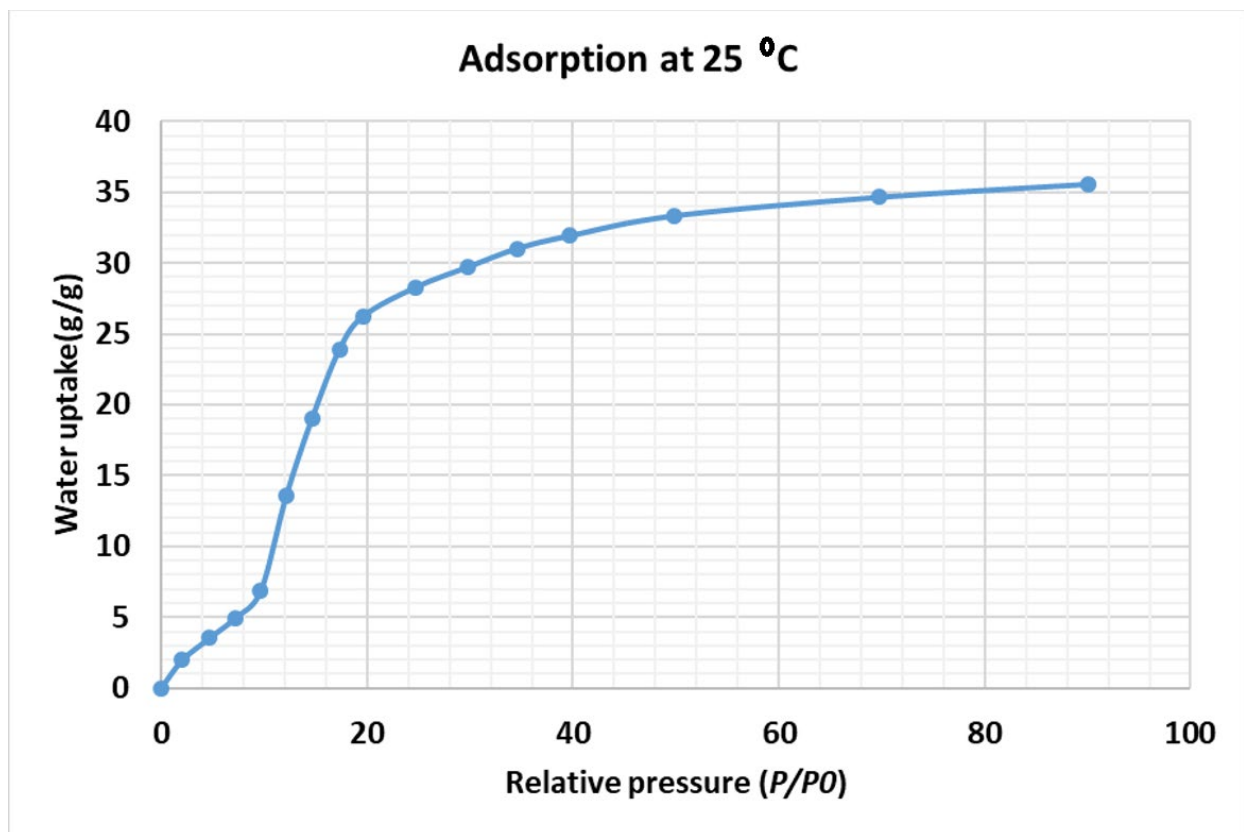


Figure 3. Water adsorption isotherm of MOF-801 nanoparticles/Graphene nanoplatelets composite at different adsorption temperatures.

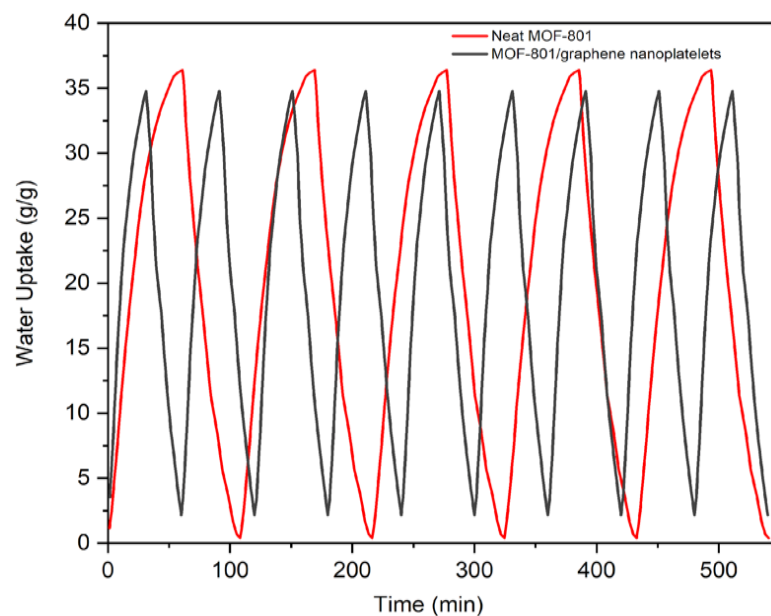


Figure 4. Cyclic performance of MOF-801/Graphene nanoparticles compared to neat MOF-801 at $P/P_0 = 0.9$ and $T_{\text{desorption}}$ of 90 °C.

Figure 5 shows the gravimetric water uptake and the kinetics of MOF-801/Graphene at different temperatures measured using a dynamic vapor sorption (DVS) analyzer [27]. Figure 5 shows that increasing the temperature results in decreasing the adsorption time and the maximum water uptake.

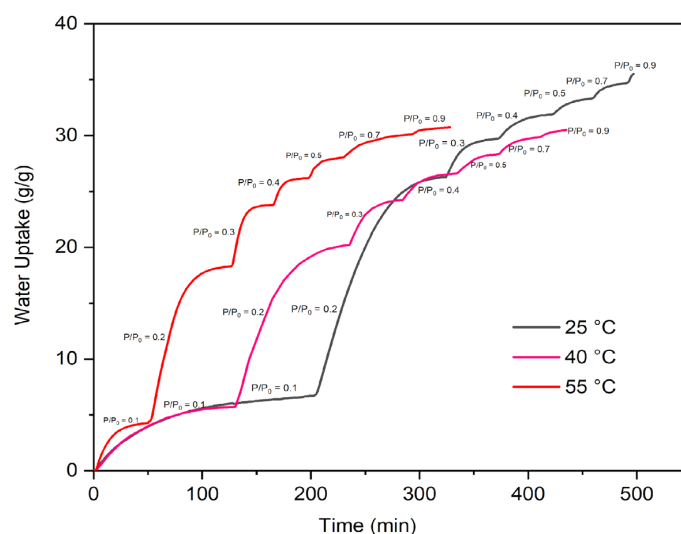


Figure 5. Water kinetics at different adsorption temperatures and relative pressures using MOF-801-G10% [27].

Using MOF-801/Graphene nanoplatelets 10% loading with enhanced water vapor adsorption characteristics, this paper describes a novel, cost-effective cooling technology for greenhouse climate control to achieve the required temperature and humidity levels. The work involves developing 3D CFD model for the water desorption and adsorption processes of MOF-801/Graphene-coated on the wire-finned heat exchanger and used to predict the best cycle time for greenhouse air dehumidification. In addition, an overall thermodynamic model of the greenhouse cooling system was developed and results from the CFD model were used to predict the overall system performance.

3. Computational Fluid Dynamic Modelling of MOF-801/Graphene

A 3D computational fluid dynamic model was developed for a copper wire finned tube heat exchanger coated with a 0.5-mm thick layer of MOF-801/Graphene. Figure 6 shows a 3D CAD drawing of this wire-finned tube which was imported to COMSOL Multiphysics to simulate the adsorption/desorption processes of water vapor on the coated MOF. In addition, this wire-finned tube was integrated with nichrome wire to provide electrical heating for the desorption process. In the COMSOL model, the following modules were used: (i) electrical heating module to simulate the heating process, (ii) heat transfer in solids and fluids module to simulate the heating effect through the body and the MOF material, (iii) Darcy's law to describe the momentum of fluid flow in the porous domain, and (iv) linear driving force (LDF) to model the MOF domain's water uptake taking into account the MOF's adsorption isotherm and kinetics.

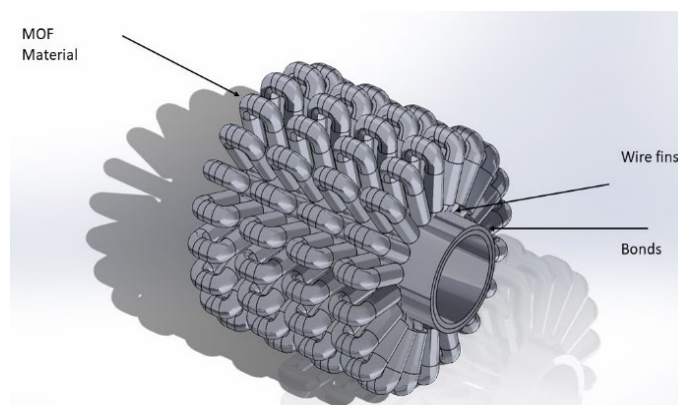


Figure 6. MOF-801/Graphene-coated wire finned tube and its 3D CAD model.

Equation (1) describes the heat transfer in solids and fluid, where Q_{ted} is the thermoelastic damping [29]

$$\rho C_p \frac{\partial T}{\partial t} + \rho C_p \mathbf{u} \nabla T + \nabla \cdot (-\mathbf{k} \cdot \nabla T) = Q_e + Q_{ted} \quad (1)$$

Equations (2)–(4) describe the electrical heating process [30].

Q_e (W/m^3) is the resistive heating in the heat equation represented in Equation (2)

$$\rho C_p \frac{\partial T}{\partial t} + \nabla \cdot (-\mathbf{k}_s \cdot \nabla T) = Q_e \quad (2)$$

J is the current density (A/m^2), and E is the electric field strength (V/m) are presented in Equations (3) and (4)

$$J = \frac{E}{Q_e} \quad (3)$$

$$E = \nabla V \quad (4)$$

Equation (5) presents the Darcy law equation [31]

$$\frac{\partial}{\partial t}(\rho \epsilon) + \nabla \cdot \left(\rho \left(\frac{-K_d}{\mu} \nabla p_v \right) \right) = Q_m \quad (5)$$

Equation (6) shows the linear driving force (LDF), where W_{inf} and W are the final and initial instantaneous water uptake, respectively [32].

$$\frac{\partial W}{\partial t} = k(W_{inf} - W) \quad (6)$$

where k is the overall mass transfer coefficient, k_0 is the LDF empirical constants, and E_a is the activation energy given by Equation (7) [23]:

$$k = k_0 e^{\left(\frac{-E_a}{RT}\right)} \quad (7)$$

The MOF permeability (K_d) is expressed as follows [33]

$$K_d = \frac{d_p^2 \epsilon^3}{150(1 - \epsilon)^2} \quad (8)$$

Q_m in Equation (9) is the mass source of the adsorbate through the adsorbent material

$$Q_m = -(1 - \epsilon) \rho_{ads} \frac{\partial W}{\partial t} \quad (9)$$

The pressure of the vapor was calculated using ideal gas as follows [34]

$$p_v = \rho_v R_v T \quad (10)$$

The equilibrium water uptake (W_{inf}) of MOF-801/Graphene was determined using Equations (11)–(14) [28–36]:

$$A = -RT \ln \left(\frac{P}{P_o} \right) \quad (11)$$

$$D_s = D_{so} e^{\left(\frac{-E_a}{RT}\right)} \quad (12)$$

$$W_{inf} = 6.88496 * e^{(-0.00081359 * A)} \text{ for } A > 3987 \quad (13)$$

$$W_{\text{inf}} = 3.9(10)^{-13}A^3 - 6.48676(10)^{-9}A^2 + 0.0000037696835A + 0.356179 \text{ for } A < 3987 \quad (14)$$

Table 1 shows the thermophysical properties of the MOF-801/Graphene used in the model.

Table 1. Thermophysical parameters [27,36].

Properties		MOF-801/Graphene
Powder particle Density		1.552 g cm ⁻³
Tortuosity		1.56
C _p values		743 J kg ⁻¹ K ⁻¹
Bulk Density		0.6 g/cm ³
Q _{st}		3300 kJ kg ⁻¹
Particle size		45–60 nm
Skeletal Density		1.77
K _d		160 W/m.k
Ea (J/mol)	D _{so} (m ² /s)	P _{ratio} (p/p _o)
27,708.06	9.00 × 10 ⁻¹⁶	P _{ratio} < 0.1
1749.93	4.00 × 10 ⁻²⁰	0.1 < P _{ratio} < 0.2
16,639.63	8.00 × 10 ⁻¹⁷	P _{ratio} > 0.2
Particle radius R _p (m)		25 × 10 ⁻⁹

All physics were coupled and solved numerically using a time-dependent solver, which solves the equations simultaneously to give accurate results with minimum solving iteration time for the non-linear equations. The initial boundary conditions are set by assuming that the adsorbent material is fully saturated with a water uptake of 0.35 kg/kg and material temperature of 30 °C. During the desorption process, the heating is enabled by applying the electrical power of 2 W for a period of 40 min. During the adsorption process, the electrical power was switched off, and the MOF-801/Graphene material was exposed to atmospheric conditions for a period of 40 min. During this simulation, a quarter of the tube is used due to symmetry at the two sides of the 3D wire finned tube.

Figure 7 shows the temperature and water uptake variation with time during one desorption and adsorption cycle with a desorption time of 40 min at an input power of 2 W, an adsorption time of 40 min at an ambient temperature of 23 °C, and humidity of 55%. The blue line represents the temperature variation with time, while the green line represents the water uptake variation with time. It can be seen that the temperature reaches a steady state after 25 min of heating, reaching 82 °C, and the water uptake decreased to 0.01 kg/kg. During the adsorption process, the water uptake increased with time till reaching an uptake of 0.17 kg/kg at 80 min.

Figures 8 and 9 show 3D images of predicted temperature and water uptake during the heating process (desorption) at 10 and 34 min and during the adsorption process at 40 and 80 min for a 15-cm wire-finned tube coated with 10 g of MOF801/Graphene. It is clear from Figure 8 that as the time increases, the temperature increases and the MOF-801/Graphene water uptake decreases, while Figure 9 shows that the water uptake increases with time during the adsorption process.

The mesh sensitivity test is carried out using the physics-controlled mesh option in COMSOL, where tetrahedron mesh shape was selected with four different sizes applied, namely extra coarse, coarse, normal, fine, and finer. Table 2 shows the number of elements used in the various options, and Figure 10 shows the predicted temperature variation with time using the four mesh sizes. It is clear that using the coarse mesh option produces similar results to the other mesh sizes but with lower computational times of 20 min. All

the simulation cases were carried out using a PC Intel core i7 processor, 48 GB RAM, 1 TB SSD Hard Drive.

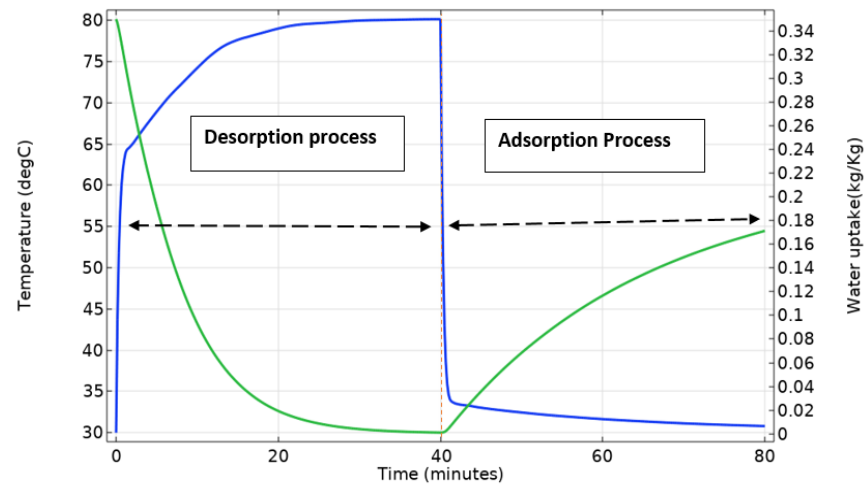


Figure 7. Simulation results at ambient operating conditions.

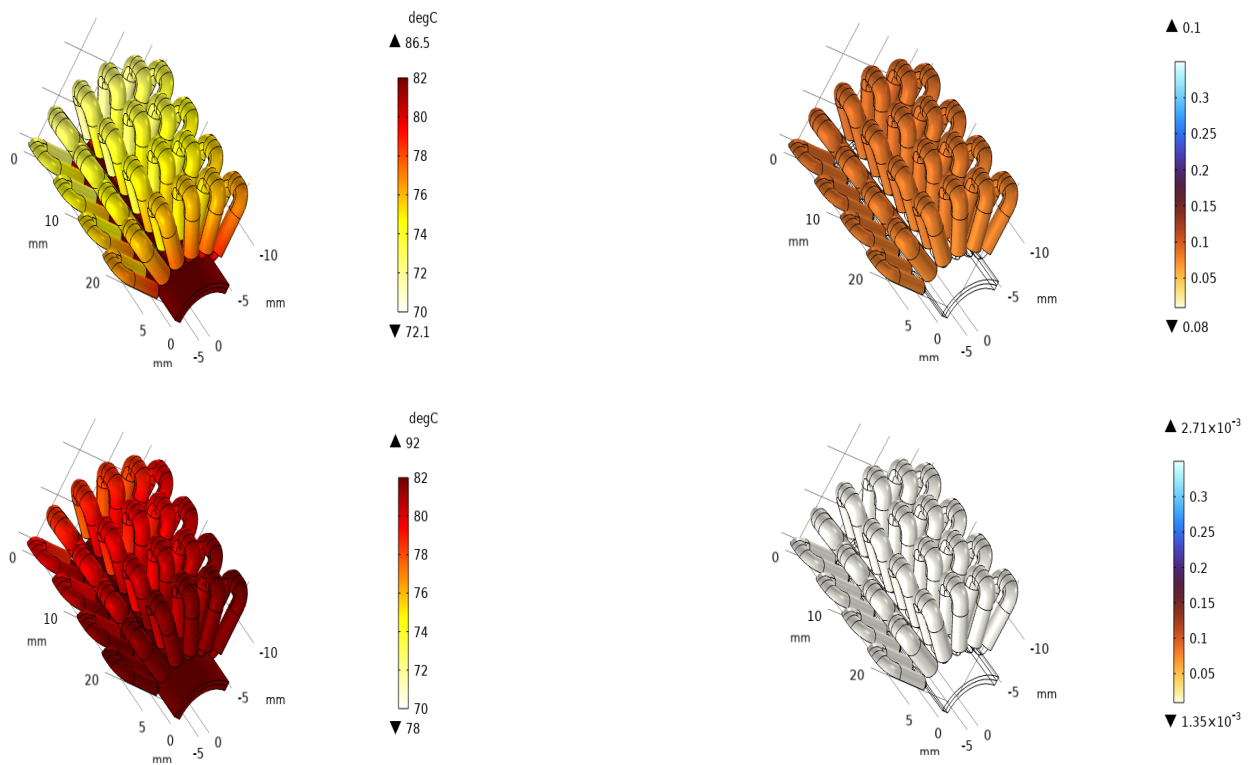


Figure 8. Shows the temperature and the water uptake variation during the desorption process for a 15 cm wire–finned tube coated with 10 g after 10, 34 min.

Table 2. Mesh sensitivity analysis.

Mesh Size	Domain Elements	Boundary Elements	Edge Elements	Simulation Time (mins)
Extra coarse	14,189	10,482	4404	14
Coarse	43,672	28,864	7128	20
Normal	87,350	50,786	10,331	30
Fine	347,294	122,756	16,041	80
Finer	806,964	208,410	21,526	127

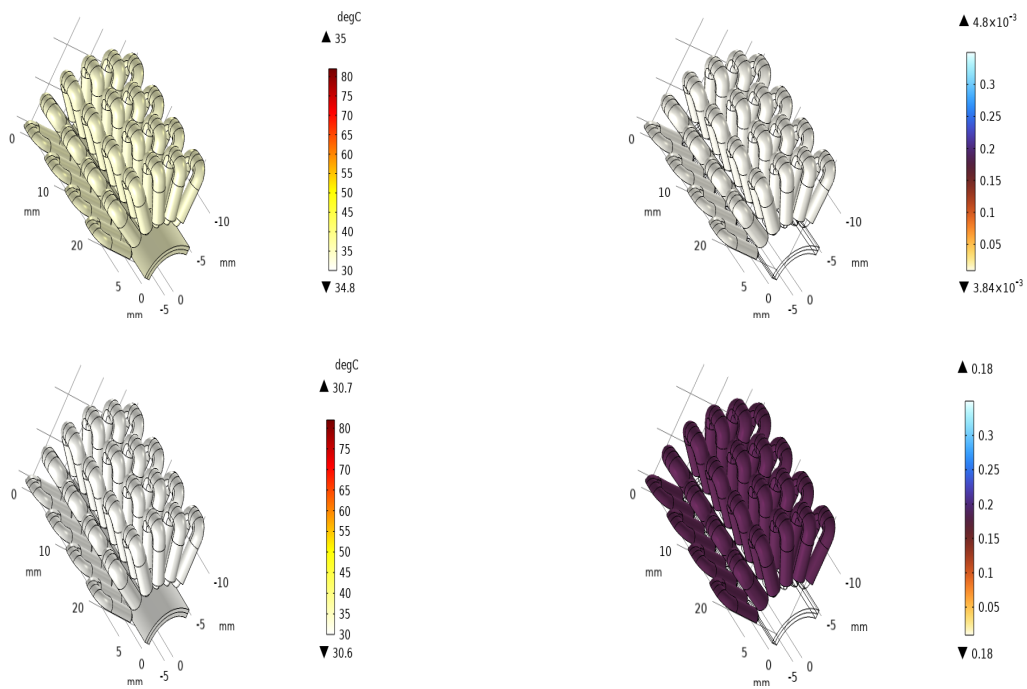


Figure 9. Shows the temperature and the water uptake variation during the adsorption process for a 15 cm wire–finned tube coated with 10 g after 40, 80 min.

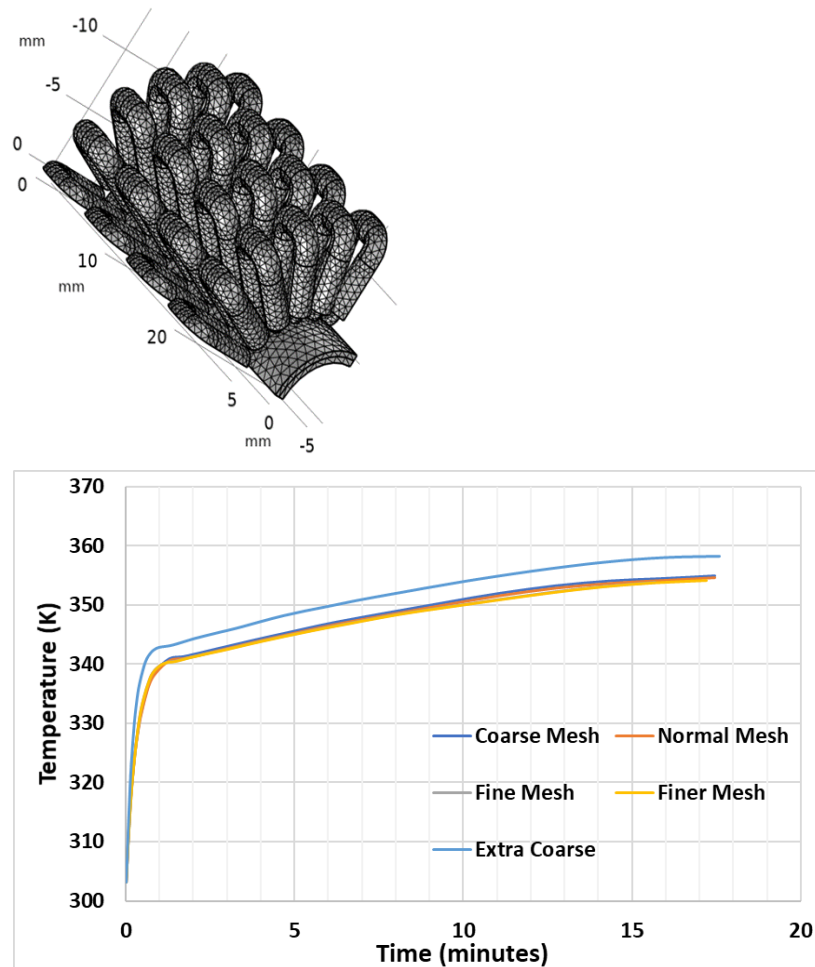


Figure 10. Mesh sensitivity analysis.

4. CFD Model Validation and Results

The modelled wire finned tube was coated with 10 g of MOF-801/Graphene using a 0.5-mm thick layer and equipped with 0.41-mm thickness Nichrome wire to provide the heating required for the desorption process. Moreover, the tube was instrumented with surface thermocouples and mounted on a sensitive scale to measure the variation of its weight with time during the desorption process due to electrical heating and the adsorption process due to moisture capture from the atmosphere, as shown in Figure 11. Tests were carried out at an ambient temperature of 23 °C and relative humidity of 55%, similar to those used in the model. Figure 12 compares the model-predicted water uptake during the adsorption process (shown in Figure 7) with the experimental measurements with time, showing good agreement with a maximum deviation of $\pm 2.35\%$. In addition, the results are repeatable with maximum deviation of 6.25%, as shown in Figure 13.

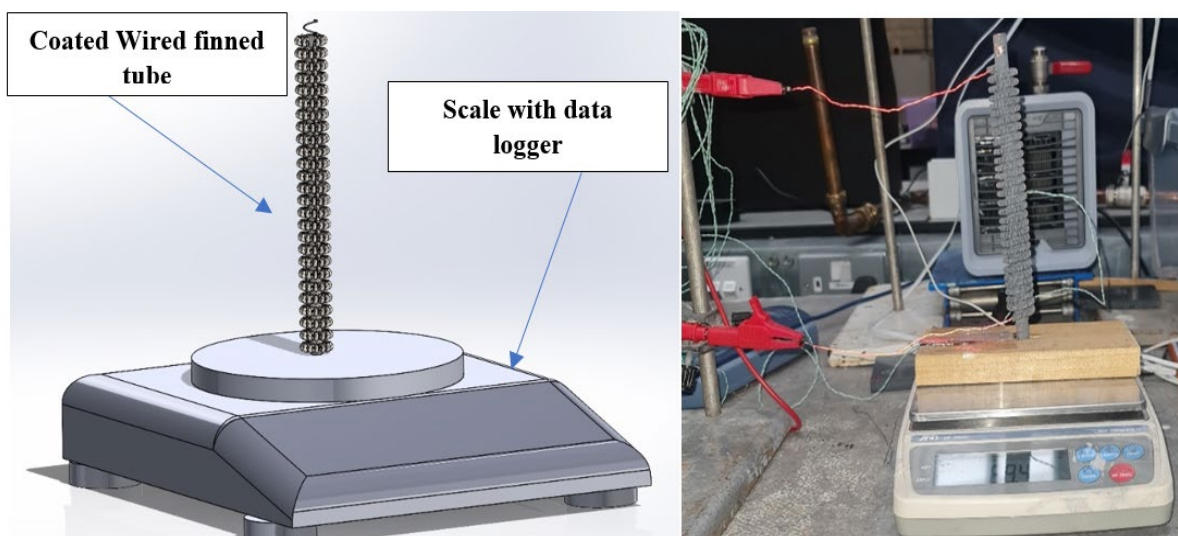


Figure 11. Validation test setup.

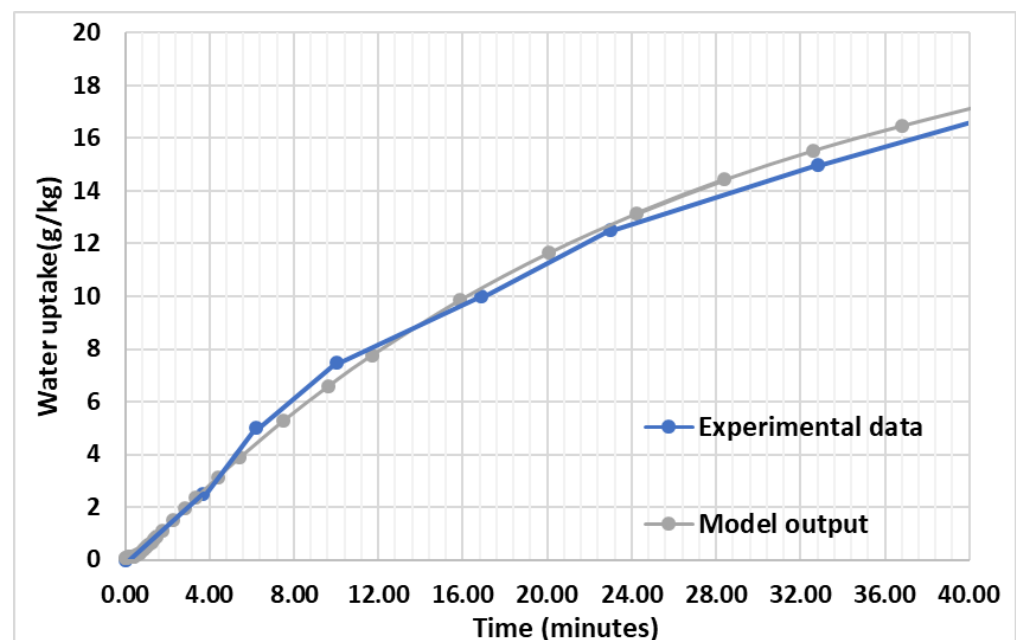


Figure 12. Comparison of the simulation results with experimental data.

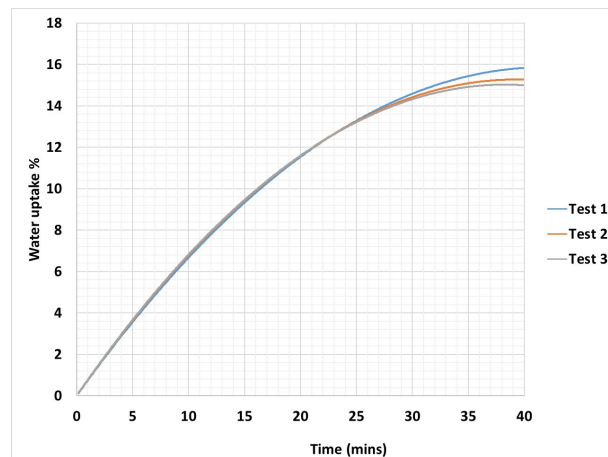


Figure 13. Repeatability test.

The validated CFD model for the adsorption/desorption cycle of MOF-801/Graphene coated on wire finned tube was used to investigate the effect of changing the desorption time (8 min, 16 min, 41 min) and the applied electrical power on the overall water uptake during the adsorption process of 44 min. Figures 14–16 show the temperature and water uptake variation with time for the power input of 1.26 W, 1.84 W, and 2 W, respectively.

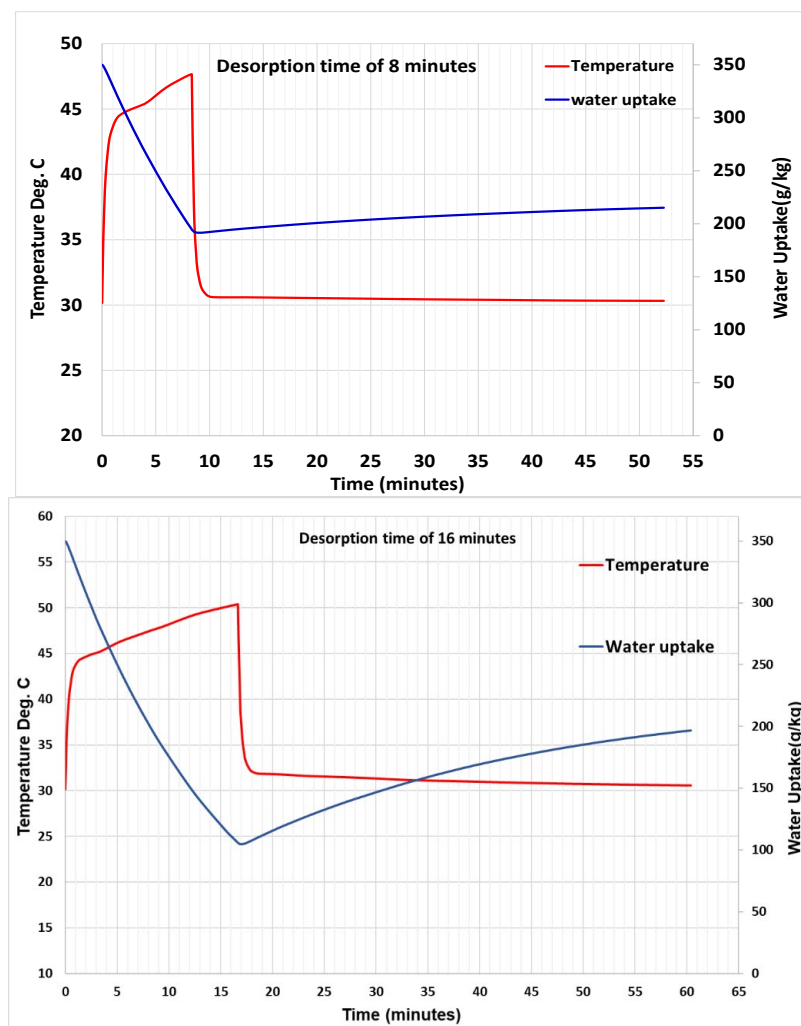


Figure 14. Cont.

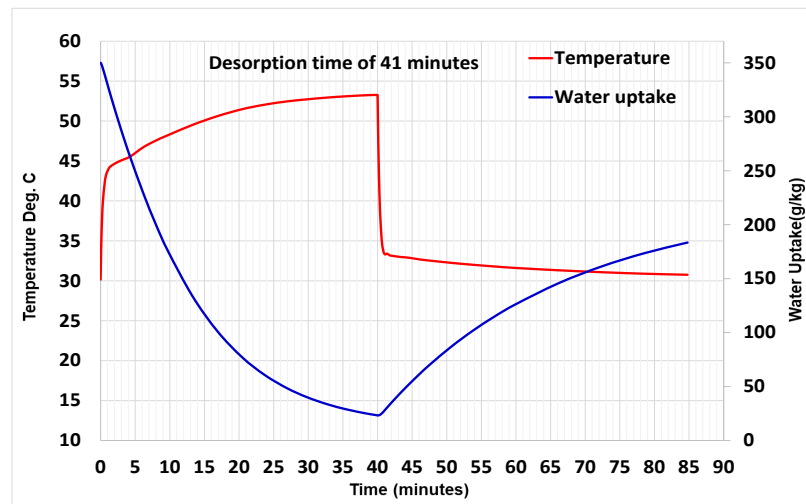


Figure 14. Temperature and water uptake variation with time during desorption and adsorption processes at input power of 1.26 W and adsorption time of 44 min.

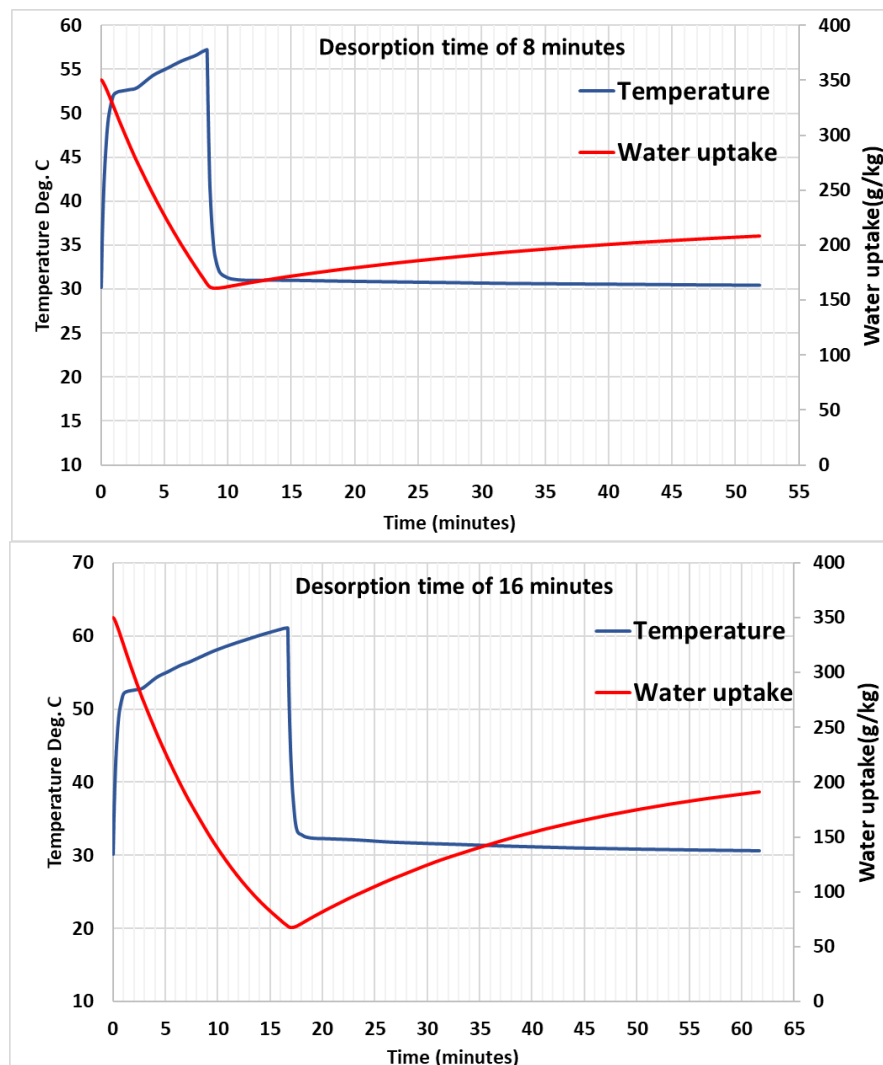


Figure 15. Cont.

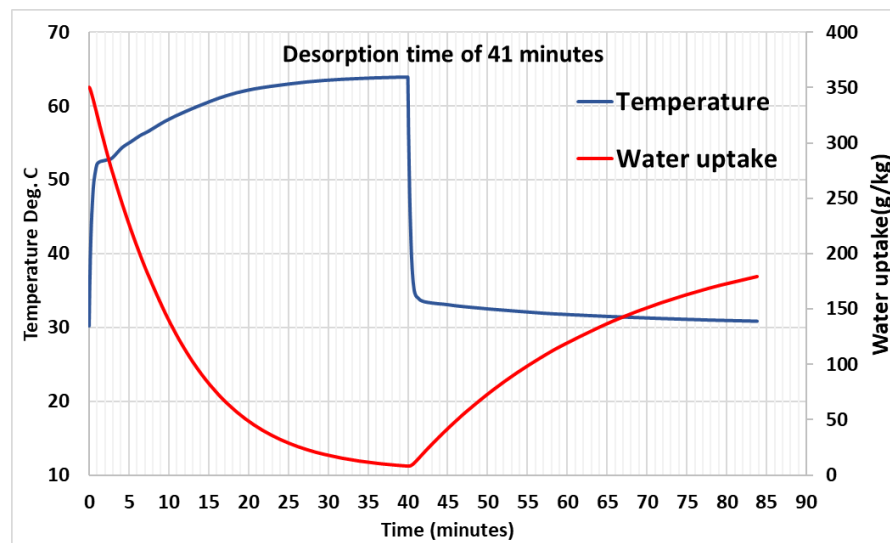


Figure 15. Temperature and water uptake variation with time during desorption and adsorption processes at input power of 1.84 W and adsorption time of 44 min.

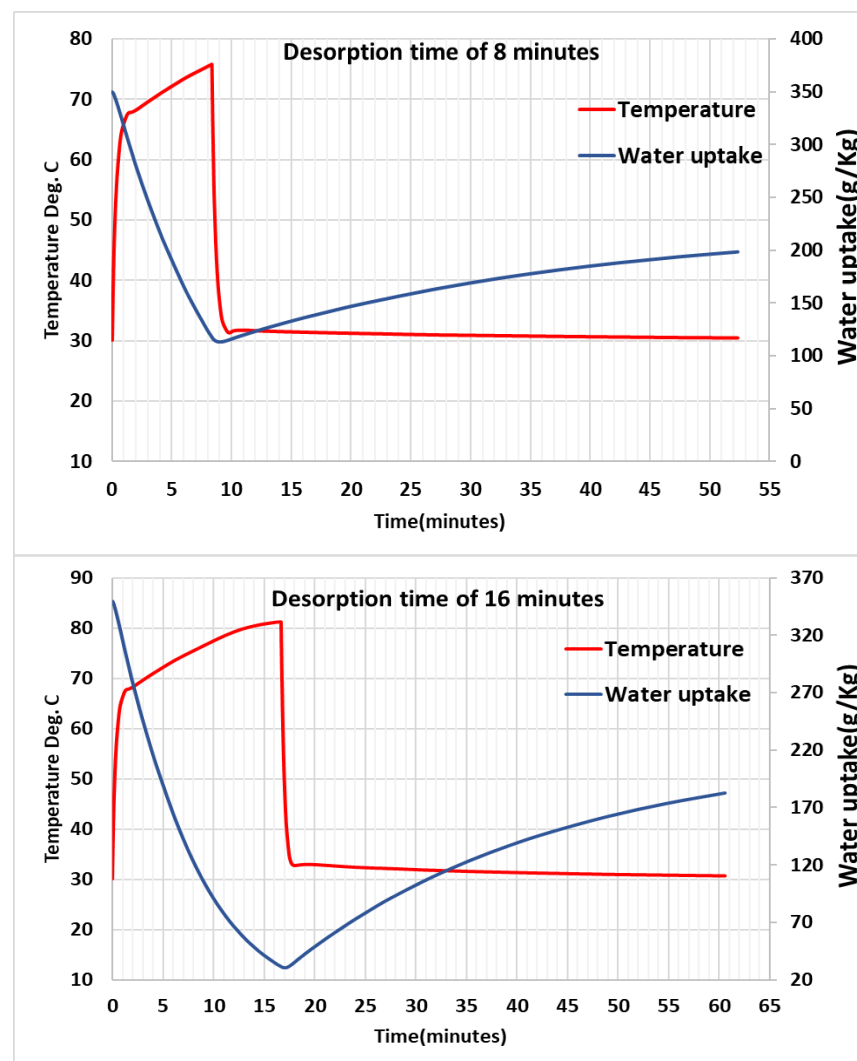


Figure 16. Cont.

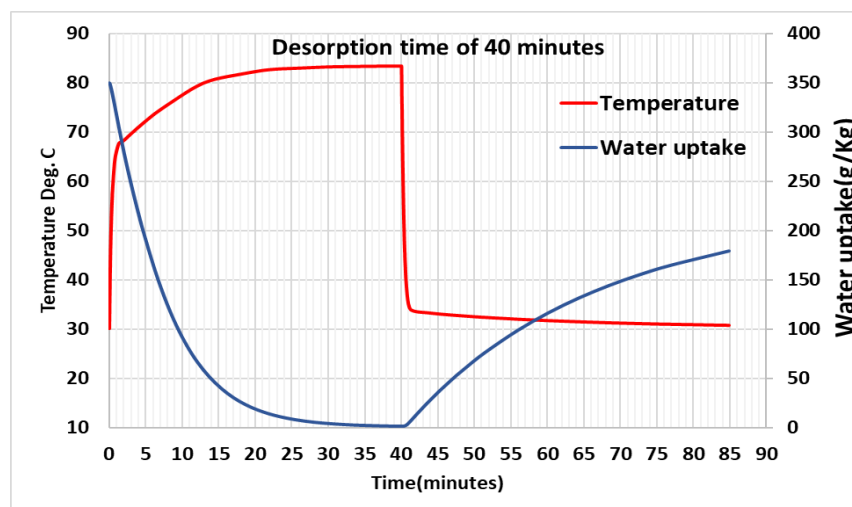


Figure 16. Temperature and water uptake variation with time during desorption and adsorption processes at input power of 2 W and adsorption time of 44 min.

Table 3 summarizes the results shown in Figures 14–16 in terms of water removal rate per cycle, number of cycles per day, total water removal per day, and the electrical power consumption per day. It is clear from this table that using a desorption time of 16 min and power input of 1.26 W can produce the highest daily water removal per power consumption of 274.42 (g/kg_{MOF})/(W.hr).

Table 3. Effect of Desorption time and power input on the daily water adsorbed and power consumption.

Power Input (W)	Desorption Time (min)	Water Uptake at End of Desorption Process (g/kg)	Water Uptake at End of Adsorption Process (g/kg)	Net Water Adsorbed per Cycle (g/kg)	Number of Cycles per Day	Net Water Adsorbed per Day (g/kg)	Power Consumption per Day (W.hr)	Water to Power Ratio (g/kg _{MOF} /W.hr)
1.26	8	191.75	215.18	23.34	27.69	648.83	4.65	139.53
	16	104.71	196.87	92.16	24.00	2211.84	8.06	274.42
	41	23.72	183.42	183.42	16.94	2705.51	14.59	185.44
1.84	8	160.00	200.00	40.00	27.69	1107.69	6.79	163.14
	16	68.60	190.00	121.40	24.00	2913.6	11.78	247.33
	41	8.00	179.00	171.00	16.94	2896.94	21.30	136.01
2	8	113.21	198.00	84.79	27.69	2348.03	11.08	211.92
	16	30.00	183.00	153.00	24.00	3672.00	19.20	191.25
	41	3.00	179.00	176.00	16.94	2981.25	34.73	85.84

5. Green House Climate Control System

Figure 17 shows a schematic diagram of the proposed greenhouse climate control system to achieve the required temperature and humidity levels. This system consists mainly of two MOF-801/Graphene-coated heat exchangers, an air-to-air heat exchanger, and an evaporative cooler that will deliver the input air at the target temperature and humidity to the greenhouse. In this system, the incoming humid air from the greenhouse at (1) will pass through the air-to-air heat exchanger to reduce the temperature of air coming from the MOF-coated heat exchanger. The air leaving the air-to-air heat exchanger (2) will pass through the MOF-801/Graphene-coated heat exchanger (DCH), where the MOF material will adsorb the air moisture content, thus reducing its humidity (3). During this process, the air temperature will increase due to the released heat of adsorption. The dehumidified hot air will then pass through the air-to-air heat exchanger where it is cooled down while its moisture content remains constant. Further cooling will be applied to the air (4) using the evaporative cooler, where the target temperature and humidity will be achieved and delivered to the greenhouse (5). In this system, two DCHs are needed to enable continuous air dehumidification, where they will alternate between adsorption and desorption processes. During the desorption process, the desorbed water vapor can be condensed in the water vapor condenser and used for irrigation of the greenhouse. D1 to D6 are dampers to control the airflow direction at various locations according to the required operating scenario.

where q_{st} is the heat of adsorption given as [38];

$$q_{st} = A = h_{fg} \left[1 + 0.2843e^{(-10.28W)} \right] \quad (21)$$

where h_{fg} is the latent heat of evaporation for water and is given by [40]:

$$h_{fg} = (2504.4 - 2.4425 T_d) \cdot 1000 \quad (22)$$

The desiccant relative humidity equation for MOF-801/Graphene:

$$\text{RHd} = 21261 \cdot W^6 - 22293 \cdot W^5 + 8844.7 \cdot W^4 - 1599.2 \cdot W^3 + 122.57 \cdot W^2 - 1.8263 \cdot W + 0.0066 \quad (23)$$

Equations (24)–(30) describe the heat transfer equations for the air-to-air heat exchanger [41]:

$$T_{po} = (T_{pi} - T_w) \cdot e^{-Ax} + T_w \quad (24)$$

$$A = \frac{-h_p \times a \times n}{m_p \times c_p} \quad (25)$$

$$R_e = \frac{V \times L}{\nu} \quad (26)$$

$$h_p = (0.664 \times (R_e^{0.5})) \times \frac{(P_r^{\frac{1}{3}} \times k)}{L} \quad (27)$$

$$A = a \times n \times \frac{\delta}{2} \quad (28)$$

$$At = n \times a \times L \quad (29)$$

$$m_p = \rho \cdot V \cdot A \quad (30)$$

Equations (31)–(45) describe the heat and mass transfer equations [42] for the evaporative cooler shown schematically in Figure 18:

$$\dot{m}_a \cdot \partial h_m = \delta \dot{Q}_S + \delta \dot{Q}_L \quad (31)$$

$$\delta \dot{Q}_S = h_T \cdot (T_w - T) \cdot \partial A \quad (32)$$

$$\delta \dot{Q}_L = \partial \dot{m}_W \cdot (C_{pv} T_w + h_{fg}) \quad (33)$$

$$\partial \dot{m}_W = h_m \cdot \rho_a (W_s - W) \quad (34)$$

$$\partial \dot{m}_W = \dot{m}_a \cdot \partial W \quad (35)$$

$$(C_{pa} + W \cdot C_{pv}) \cdot \frac{\partial T}{\partial x} = \left[\frac{P \cdot h_T}{\dot{m}_a} + C_{pv} \cdot \frac{\partial W}{\partial x} \right] \cdot (T_w - T) \quad (36)$$

$$\frac{\partial W}{\partial x} \dot{m}_a = P \cdot h_m \cdot \rho_a (W_s - W) \quad (37)$$

$$R_e = \frac{U \cdot D_h}{\nu_a} \quad (38)$$

$$D_h = 2 \cdot D \quad (39)$$

$$\text{Nu} = \text{Sh} = 7.54 \quad (40)$$

$$h_T = \frac{D_{va} \cdot \text{Sh}}{D_h} \quad (41)$$

$$h_m = \frac{k_a \cdot \text{Nu}}{D_h} \quad (42)$$

$$D_{va} = 1.87 \cdot 10^{-10} \cdot T^{2.072} \quad (43)$$

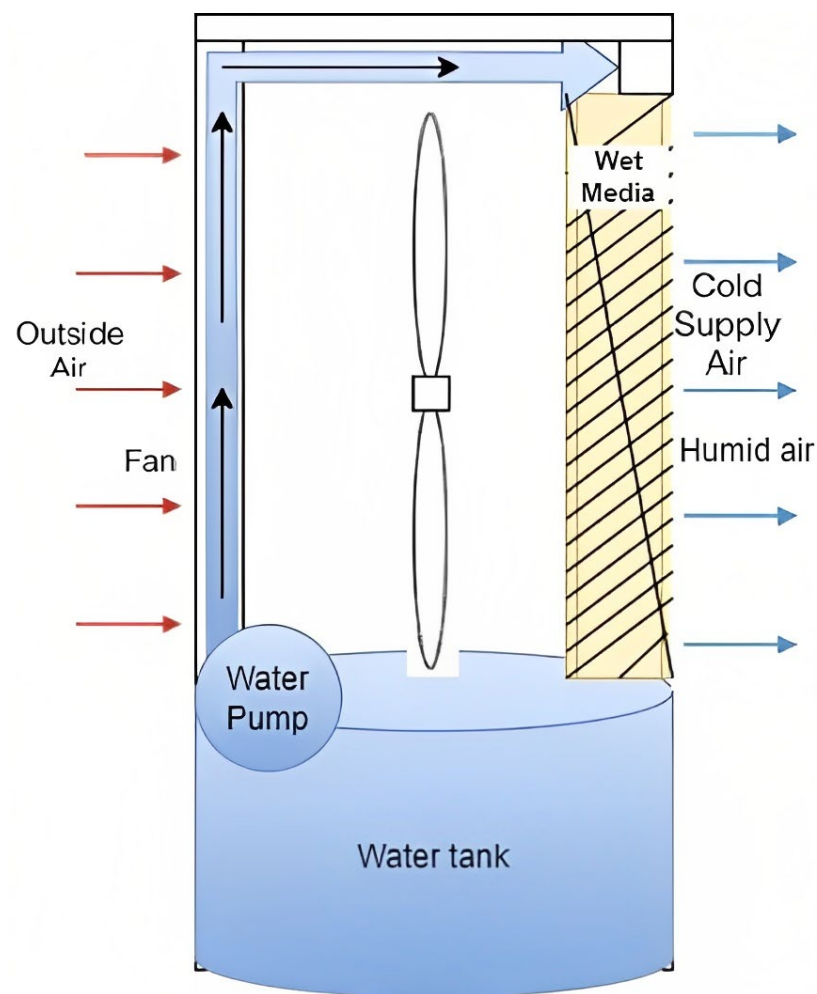


Figure 18. Schematic diagram of direct evaporative cooler.

Boundary condition

$$T_W = T_{wb}(T_{in}, \varphi_{in}) \quad (44)$$

$$W_s = W(T_w, \varphi = 100\%) \quad (45)$$

The above equations for the DCHs, air-to-air heat exchanger, and evaporative cooler are solved using MATLAB according to the flow chart in Figure 19 using the inputs listed in Table 4 coupled with CoolProp [43] for air properties.

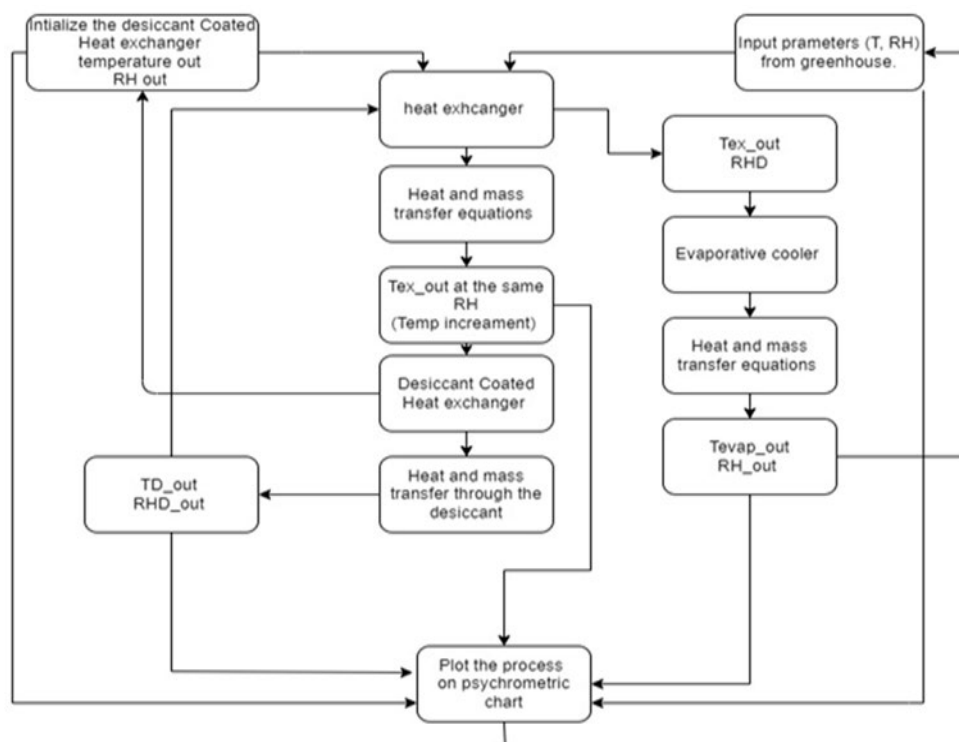


Figure 19. The flow chart of the integrated cycle for the greenhouse climate control system.

Table 4. Input parameters to the greenhouse climate control system.

Model Inputs	Value	Units
Air relative humidity (RH _{air})	65, 75, 90	%
Air temperature (T _{air})	30	°C
Air velocity (U)	1.5, 2.5, 3.5	m/s
Air density (Roh _{air})	1.2	kg/m ³
Desiccant density (Roh _{desiccant})	600	kg/m ³
Sher wood number (Sh)	2.5	-
Specific heat of air	1005	kJ/kg/K
Air Thermal conductivity	0.175	W/mK
Nusselt number	2.45	-
The thickness of plates (t)	0.4	m
Length of plates (L)	0.6	m
Width of plates (a)	0.4	m
Channel width (sigma)	4 × 10 ⁻³	m
No of plates	70	-
Total heat exchange area (At)	16.8	m ²
Prandtl number (Pr)	0.711	-
Dynamic viscosity (neu)	16.97 × 10 ⁻⁶	Ns/m

The submodels of the major components of the system, such as the DCHs, the air-to-air heat exchanger, and the evaporative cooler, were validated using published literature. Table 5 presents the results of validating the evaporative cooler submodel using three conditions at T = 40 °C and relative humidity 30%, 50% and 70%. The direct evaporative cooler model’s outputs agree with published modelling and experimental data by Igor Kovačević [42], with a maximum difference of less than 1% for output temperature and relative humidity.

Table 5. Evaporative cooler model validation.

Case 1				
Parameter	Inputs	Current Model Outputs	Published Data	Experimental
Temperature (°C)	40	25.13	25.34	25.3
Relative humidity	30%	97.16%	97.16%	97.16%
Specific humidity (g/g)	13.9	19.7	19.9	19.9
Case 2				
Parameter	Inputs	Model outputs	Published data	experimental
Temperature (°C)	40	30.33	30.47	30.5
Relative humidity	50%	98.46%	98.46%	98.46%
Specific humidity (g/g)	23.5	27.3	27.5	27.6
Case 3				
Parameter	Inputs	Model outputs	Published data	experimental
Temperature (°C)	40	34.65	34.72	n/a
Relative humidity	70%	99.12%	99.12%	n/a
Specific humidity (g/g)	33.4	35.51	35.6	27.6

The air-to-air heat exchanger submodel was validated using published results of R. S. Bindu [41] with no deviation, as shown in Figure 20.

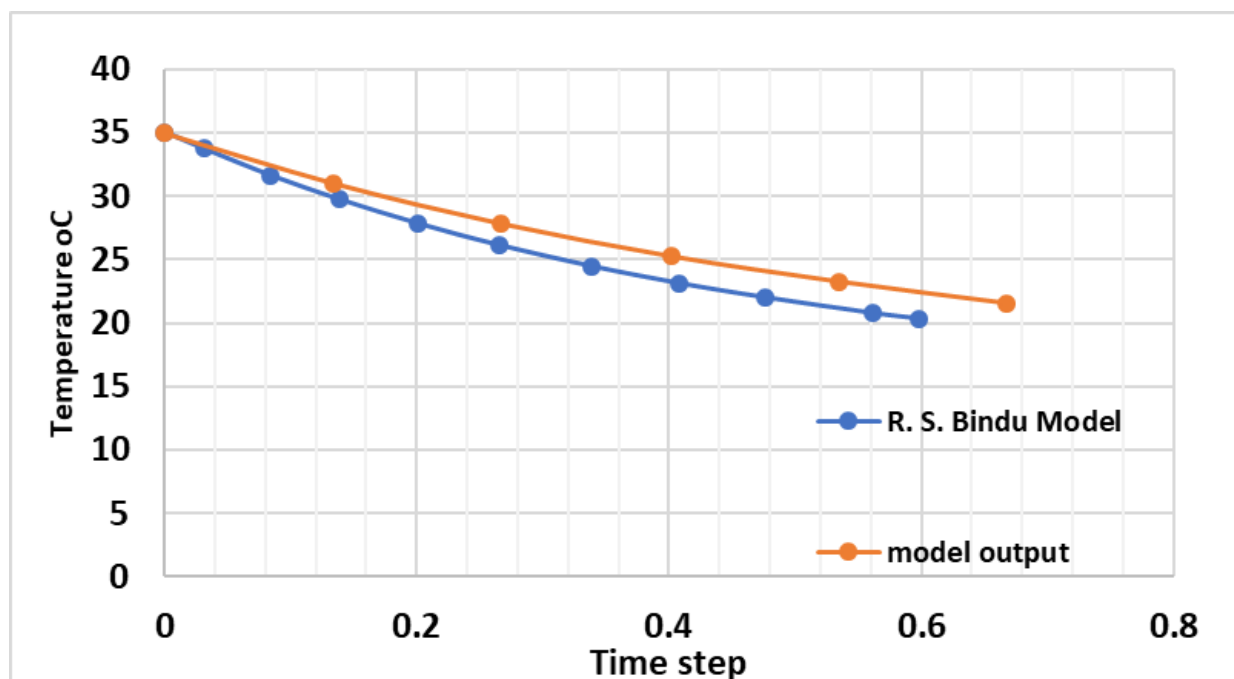
**Figure 20.** Air-to-air heat exchanger model validation.

Figure 21 compares the desiccant-coated heat exchanger submodel results to those published by Yadav et al. [36], showing good agreement with a maximum deviation of 13%.

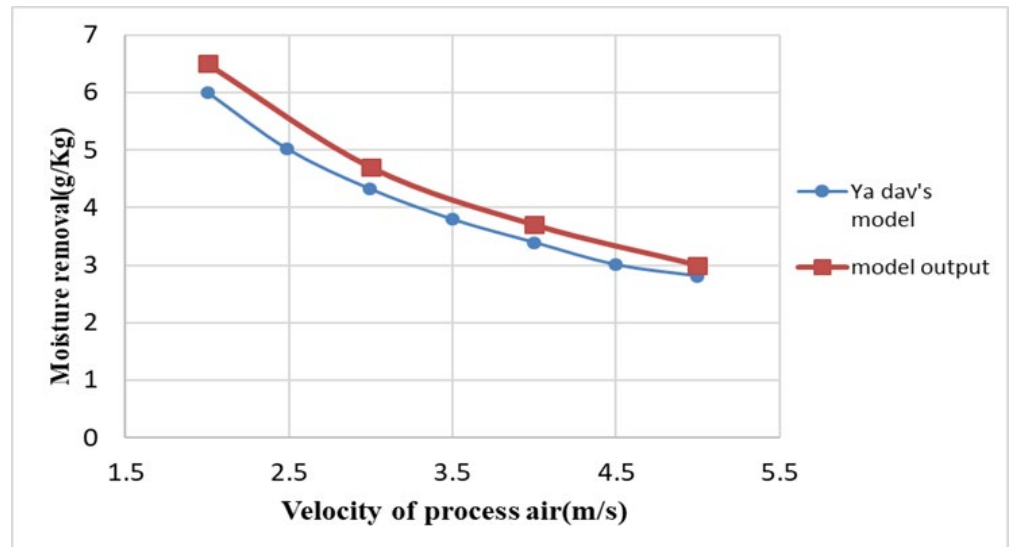


Figure 21. DCHE model validation.

6. Overall System Performance Results

The above-developed model for the greenhouse climate control system was used to predict its performance in the case of a greenhouse with initial conditions of 30 °C temperature and 90% relative humidity. For the MOF DCH, the initial condition of the MOF material was obtained from the CFD analysis where the temperature and water uptake of the desiccant are 50 °C and 0.104 kg/kg. These conditions were achieved using the desorption time of 16 min and a power input of 1.26 W with the highest water removal rate per unit power consumption. Figure 22 shows the psychrometric chart for the air as it flows through various parts of the system where the air coming from the greenhouse is heated up in the air to air heat exchanger from 30 °C to 41 °C. Then, the hot and humid air will pass through the MOF DCH, where the specific humidity of the air is reduced significantly from 24.27 g/kg to 7.86 g/kg. As the dehumidified and hot air flows through the air-to-air heat exchanger, its temperature will decrease from 41 °C to 36.91 °C. In the evaporative cooler, the dehumidified and hot air is further cooled and humidified to achieve the target air temperature and relative humidity of 25 °C and 40%, respectively, at the inlet to the greenhouse.

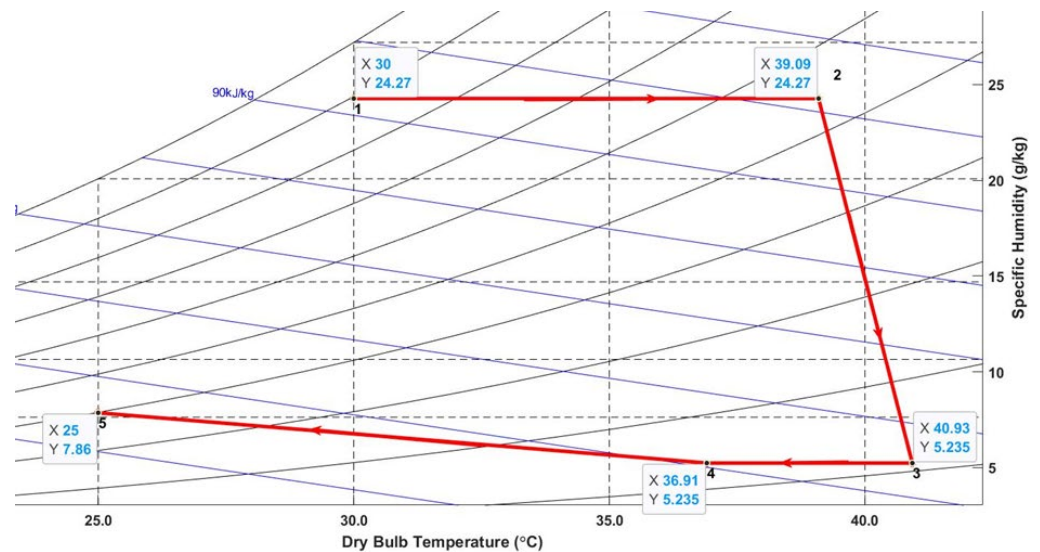


Figure 22. Psychrometric chart output.

Figure 23 shows the effect of changing the relative humidity inside the greenhouse at 65%, 75%, and 90% and its impact on the system performance. By increasing the relative humidity value at point (1) from 65% to 75% and then to 90%, the specific humidity for the air at point (5) increased from 5.78 g/kg to 7 g/kg, and then to 7.8 g/kg, respectively. Using 16 min of heating (desorption) and 44 min of adsorption, the total number of cycles/day is 24, leading to the production of 4.42 liters of water per day collected from the two DCHes used in this system.

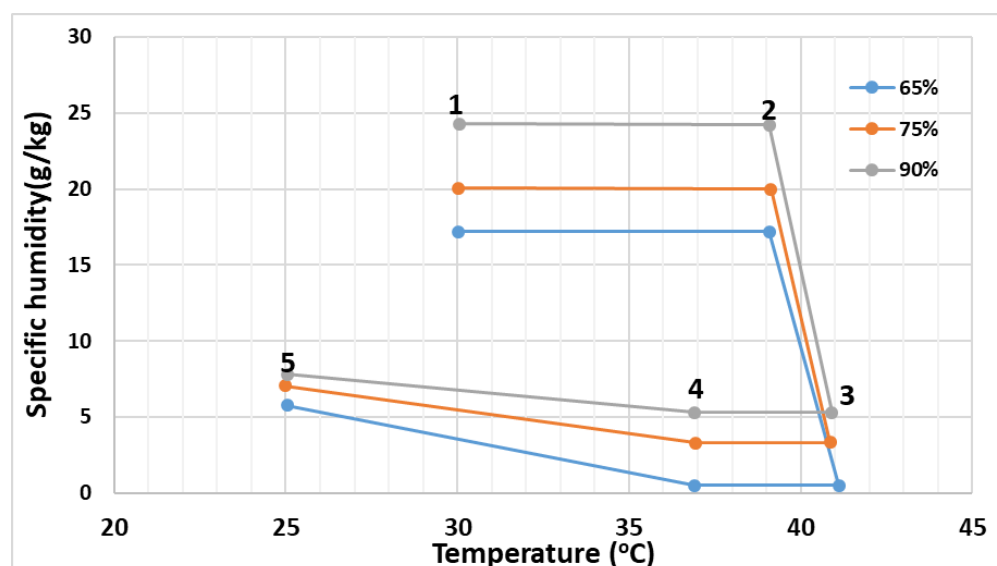


Figure 23. Inlet velocity change for the desiccant wheel and studies its effect on the system behaviour on a psychrometric chart.

7. Conclusions

Food security depends on adequate crop production, which is adversely affected by the extreme temperatures in hot climates, lack of irrigation water, and poor soil quality. Greenhouses with controlled environment can enhance food security, particularly in areas with high temperature and water scarcity, by growing crops throughout the year independently from weather conditions. In this paper, a novel system for greenhouse climate control was developed using a metal–organic framework-based desiccant coated heat exchanger integrated with an air-to-air heat exchanger and evaporative cooler. Coupled with this model, computational fluid dynamics modelling for MOF-801/Graphene coated heat exchanger was developed to predict the best desorption time and power consumption. Results showed that:

1. Adding graphene nanoplatelets to the synthesis of MOF-801 creates nucleating surfaces where the MOFs particles adhere to the forming MOF-801/Graphene composite. The MOF-801/Graphene is highly porous with enhanced water sorption kinetics and cyclic performance, but with a slight decrease in the water uptake and enhanced thermal stability.
2. MOF-801/Graphene with 10% graphene is the most appropriate ratio since increasing the graphene percentage by more than 10% will decrease the surface area to half ($420 \text{ m}^2/\text{g}$ in the case of 20% graphene).
3. The CFD modelling of MOF-801/Graphene coated on wire finned heat exchanger showed that using power input of 1.26 W and desorption time of 16 min, the MOF-801/Graphene coated heat exchanger produces the highest water removal rate per unit power consumption of $274.42 \text{ g}/\text{kg}_{\text{MOF}}/\text{W}\cdot\text{hr}$.
4. The developed system can handle greenhouses' high relative humidity of 90% and achieve the target return air relative humidity of 50%. Similarly, the system can achieve

- other desired return air conditions starting from different greenhouse relative humidity.
5. Reducing the air velocity through the system showed advantages in terms of achieving lower relative humidity at the return to the greenhouse. For example, with air velocity of 3.5 m/s, the specific humidity of the return air is 10.5 g/kg while at the velocity of 1.5 m/s, the return air specific humidity is 3.7 g/kg.
 6. The developed system shows the ability to recover the water from reducing the greenhouse relative humidity to be used either for irrigation or any other applications. The daily water recovery is found to be 4.4 liter/kg_{MOF} used.

Author Contributions: Conceptualization, R.A.-D., S.M., M.A.I., M.K.A., M.F.E.-K. and H.S.; methodology, A.N.A.; software, A.N.A.; validation, A.N.A.; formal analysis, A.N.A.; investigation, A.N.A.; resources, R.A.-D.; data curation, A.N.A.; writing—original draft preparation, A.N.A.; writing—review and editing, R.A.-D., S.M., M.A.I., M.K.A., M.F.E.-K. and H.S.; visualization, R.A.-D., S.M., M.A.I., M.K.A., M.F.E.-K. and H.S.; supervision, R.A.-D. and S.M.; project administration, R.A.-D. and S.M.; funding acquisition, R.A.-D., S.M., M.A.I., M.K.A., M.F.E.-K. and H.S. All authors have read and agreed to the published version of the manuscript.

Funding: This research was funded by [the Deanship of Scientific Research at King Khalid University for funding this work through research group program] grant number [GP.1/308/43], Also was funded by [the British Council for their support under Research Environment Links call for project entitled capacity building in Egypt for enhancing water availability, food security and renewable energy using MOF adsorption heat pumps] grant number [871105921], and The APC was funded by [the British Council grant number 871105921].

Institutional Review Board Statement: Not applicable.

Informed Consent Statement: Not applicable.

Data Availability Statement: Not applicable.

Acknowledgments: The authors extend their appreciation to the Deanship of Scientific Research at King Khalid University for funding this work through research group program under grant number GP.1/308/43. Also, the authors would like to thank the British Council for their support under Research Environment Links call for project entitled “Capacity building in Egypt for enhancing water availability, food security and renewable energy using MOF adsorption heat pumps (Grants no. 871105921). The authors also would like to acknowledge the support provided by Newton-Mosharafa fund from the Ministry of Higher Education of the Arab Republic of Egypt and the British council.

Conflicts of Interest: The authors declare no conflict of interest.

References

1. Wilmoth, J.; Menozzi, C.; Bassarsky, L. *Why Population Growth Matters for Sustainable Development*; United Nations: New York, NY, USA, 2022; pp. 1–4. Available online: https://www.un.org/development/desa/pd/sites/www.un.org.development.desa.pd/files/undesapd_2022_policy_brief_population_growth.pdf (accessed on 1 March 2023).
2. Li, M.; Guo, Z.; Zhang, W. Balancing food security and environmental sustainability by optimizing seasonal-spatial crop production in Bangladesh. *Environ. Res. Lett.* **2021**, *16*, 074046. [[CrossRef](#)]
3. Soussi, M.; Chaibi, M.T.; Buchholz, M.; Saghrouni, Z. Comprehensive Review on Climate Control and Cooling Systems in Greenhouses under Hot and Arid Conditions. *Agronomy* **2022**, *12*, 626. [[CrossRef](#)]
4. Ghoulem, M.; El Moueddeb, K.; Nehdi, E.; Boukhanouf, R.; Kaiser Calautit, J. Greenhouse design and cooling technologies for sustainable food cultivation in hot climates: Review of current practice and future status. *Biosyst. Eng.* **2019**, *183*, 121–150. [[CrossRef](#)]
5. Amani, M.; Foroushani, S.; Sultan, M.; Bahrami, M. Comprehensive review on dehumidification strategies for agricultural greenhouse applications. *Appl. Therm. Eng.* **2020**, *181*, 115979. [[CrossRef](#)]
6. Villarreal-Guerrero, F.; Kacira, M.; Fitz-Rodríguez, E.; Linker, R.; Kubota, C.; Giacomelli, G.A.; Arbel, A. Simulated performance of a greenhouse cooling control strategy with natural ventilation and fog cooling. *Biosyst. Eng.* **2012**, *111*, 217–228. [[CrossRef](#)]
7. Yang, Y.; Guo, S.; Chen, Y. Estimated viability of greenhouse cooling technologies for growing a tomato crop under various climates. *Int. J. Agric. Biol. Eng.* **2021**, *14*, 90–95. [[CrossRef](#)]

8. Gorjian, S.; Calise, F.; Kant, K.; Ahamed, M.S.; Copertaro, B.; Najafi, G.; Zhang, X.; Aghaei, M.; Shamshiri, R.R. A review on opportunities for implementation of solar energy technologies in agricultural greenhouses. *J. Clean. Prod.* **2021**, *285*, 124807. [CrossRef]
9. Buchholz, M. The new generation of greenhouses. In *Unlocking the Potential of Protected Agriculture in the Countries of the Gulf Cooperation Council—Saving Water and Improving Nutrition*; FAO: Cairo, Egypt, 2021; ISBN 9789251341919. Available online: <https://www.ptonline.com/articles/how-to-get-better-mfi-results> (accessed on 1 March 2023).
10. Buker, M.S.; Riffat, S.B. Recent developments in solar assisted liquid desiccant evaporative cooling technology—A review. *Energy Build.* **2015**, *96*, 95–108. [CrossRef]
11. Davies, P.A.; Zaragoza, G. Ideal performance of a self-cooling greenhouse. *Appl. Therm. Eng.* **2019**, *149*, 502–511. [CrossRef]
12. Amani, M.; Bahrami, M. Greenhouse dehumidification by zeolite-based desiccant coated heat exchanger. *Appl. Therm. Eng.* **2021**, *183*, 116178. [CrossRef]
13. Sultan, M.; Miyazaki, T.; Saha, B.B.; Koyama, S. Steady-state investigation of water vapor adsorption for thermally driven adsorption based greenhouse air-conditioning system. *Renew. Energy* **2016**, *86*, 785–795. [CrossRef]
14. Vivekh, P.; Kumja, M.; Bui, D.T.; Chua, K.J. Recent developments in solid desiccant coated heat exchangers—A review. *Appl. Energy* **2018**, *229*, 778–803. [CrossRef]
15. Ghali, K. Energy savings potential of a hybrid desiccant dehumidification air conditioning system in Beirut. *Energy Convers. Manag.* **2008**, *49*, 3387–3390. [CrossRef]
16. Saeed, A.; Al-Alili, A. A review on desiccant coated heat exchangers. *Sci. Technol. Built Environ.* **2017**, *23*, 136–150. [CrossRef]
17. Ge, T.S.; Zhang, J.Y.; Dai, Y.J.; Wang, R.Z. Experimental study on performance of silica gel and potassium formate composite desiccant coated heat exchanger. *Energy* **2017**, *141*, 149–158. [CrossRef]
18. Valarezo, A.S.; Sun, X.Y.; Ge, T.S.; Dai, Y.J.; Wang, R.Z. Experimental investigation on performance of a novel composite desiccant coated heat exchanger in summer and winter seasons. *Energy* **2019**, *166*, 506–518. [CrossRef]
19. Hu, L.M.; Ge, T.S.; Jiang, Y.; Wang, R.Z. Performance study on composite desiccant material coated fin-tube heat exchangers. *Int. J. Heat Mass Transf.* **2015**, *90*, 109–120. [CrossRef]
20. AL-Dadah, R.; Mahmoud, S.; Elsayed, E.; Youssef, P.; Al-Mousawi, F. Metal-organic framework materials for adsorption heat pumps. *Energy* **2020**, *190*, 116356. [CrossRef]
21. Youssef, P.G.; Dakkama, H.; Mahmoud, S.M.; AL-Dadah, R.K. Experimental investigation of adsorption water desalination/cooling system using CPO-27Ni MOF. *Desalination* **2017**, *404*, 192–199. [CrossRef]
22. Rezk, A.; Al-Dadah, R.; Mahmoud, S.; Elsayed, A. Characterisation of metal organic frameworks for adsorption cooling. *Int. J. Heat Mass Transf.* **2012**, *55*, 7366–7374. [CrossRef]
23. Elsayed, E.M.; Hussein, A. Numerical and Experimental Evaluation of Advanced Metal-Organic Framework Materials for Adsorption Heat Pumps. Ph.D. Thesis, University of Birmingham, Birmingham, UK, 2018.
24. Liu, X.; Wang, X.; Kapteijn, F. Water and Metal-Organic Frameworks: From Interaction toward Utilization. *Chem. Rev.* **2020**, *120*, 8303–8377. [CrossRef] [PubMed]
25. Taddei, M.; McPherson, M.J.; Gougsa, A.; Lam, J.; Sewell, J.; Andreoli, E. An optimised compaction process for zr-fumarate (MOF-801). *Inorganics* **2019**, *7*, 110. [CrossRef]
26. Solovyeva, M.V.; Gordeeva, L.G.; Krieger, T.A.; Aristov, Y.I. MOF-801 as a promising material for adsorption cooling: Equilibrium and dynamics of water adsorption. *Energy Convers. Manag.* **2018**, *174*, 356–363. [CrossRef]
27. Diab, K.; Albaik, I.; Al-Dadah, R.; Mahmoud, S.; A Ismail, M.; K Almesfer, M.; Elkady, M.; Abdelmoneim, A. Enhancing the Water Sorption Kinetics and Thermophysical Properties of Zirconium Metal-Organic Frameworks for More Efficient Sorption-Driven Applications. *SSRN Electron. J.* **2022**. [CrossRef]
28. Visa, A.; Maranescu, B.; Bucur, A.; Iliescu, S.; Demadis, K.D. Synthesis and characterization of a novel phosphonate metal organic framework starting from copper salts. *Phosphorus Sulfur Silicon Relat. Elem.* **2014**, *189*, 630–639. [CrossRef]
29. Multiphysics, C. Heat Transfer Module. © 1998–2018 Comsol 2015, pp. 1–222. Available online: <https://doc.comsol.com/5.4/doc/com.comsol.help.heat/HeatTransferModuleUsersGuide.pdf> (accessed on 1 March 2023).
30. COMSOL Multiphysics AC/DC Module User’s Guide. © 1998–2019 Comsol 2019, p. 300. Available online: <https://doc.comsol.com/5.4/doc/com.comsol.help.acdc/ACDCModuleUsersGuide.pdf> (accessed on 1 March 2023).
31. Tun, H.; Chen, C.C. Isotheric heat of adsorption from thermodynamic Langmuir isotherm. *Adsorption* **2021**, *27*, 979–989. [CrossRef]
32. Rezk, A. Theoretical and Experimental Investigation of Silica Gel/Water Adsorption Refrigeration Systems. Ph.D. Thesis, University of Birmingham, Birmingham, UK, 2012.
33. Solmuş, I.; Yamali, C.; Yildirim, C.; Bilen, K. Transient behavior of a cylindrical adsorbent bed during the adsorption process. *Appl. Energy* **2015**, *142*, 115–124. [CrossRef]
34. Lampinen, M.J. *Thermodynamics of Humid Air*; Ene-39.4027-Mass Transf. P; Department of Energy Technology, Aalto University: Espoo, Finland, 2015; p. 39.
35. Albaik, I.; Diab, K.; Al-Dadah, R.; Mahmoud, S.; Ismail, M.A. Coating Thickness Effect on the Cyclic Performance of Aluminum and Zirconium Metal-Organic Frameworks for Heat Pump Application. *Int. Conf. Appl. Energy* **2021**, *22*, 1–6. [CrossRef]
36. Albaik, I. Numerical and Experimental Development of an Efficient Adsorption Desalination and Cooling System. Ph.D. Thesis, University of Birmingham, Birmingham, UK, 2022.

37. Ge, T.S.; Li, Y.; Wang, R.Z.; Dai, Y.J. A review of the mathematical models for predicting rotary desiccant wheel. *Renew. Sustain. Energy Rev.* **2008**, *12*, 1485–1528. [[CrossRef](#)]
38. Yadav, A.; Yadav, L. Comparative performance of desiccant wheel with effective and ordinary regeneration sector using mathematical model. *Heat Mass Transf. Stoffuebertragung* **2014**, *50*, 1465–1478. [[CrossRef](#)]
39. San, J.Y.; Hsiau, S.C. Effect of axial solid heat conduction and mass diffusion in a rotary heat and mass regenerator. *Int. J. Heat Mass Transf.* **1993**, *36*, 2051–2059. [[CrossRef](#)]
40. Aziz, A.N.; Mahmoud, S.; Al-Dadah, R.; Ismail, M.A.; Al Mesfer, M.K. Numerical and experimental investigation of desiccant cooling system using metal organic framework materials. *Appl. Therm. Eng.* **2022**, *215*, 118940. [[CrossRef](#)]
41. Bindu, R.S.; Neeraj Kumar, A.N.; Choudhary, N.; Gupta, P. Design of Indirect Evaporative Cooler. *Int. J. Eng. Res.* **2017**, *V6*, 253–260. [[CrossRef](#)]
42. Kovačević, I.; Sourbron, M. The numerical model for direct evaporative cooler. *Appl. Therm. Eng.* **2017**, *113*, 8–19. [[CrossRef](#)]
43. Bell, I.H.; Wronski, J.; Quoilin, S.; Lemort, V. Pure and pseudo-pure fluid thermophysical property evaluation and the open-source thermophysical property library coolprop. *Ind. Eng. Chem. Res.* **2014**, *53*, 2498–2508. [[CrossRef](#)]

Disclaimer/Publisher’s Note: The statements, opinions and data contained in all publications are solely those of the individual author(s) and contributor(s) and not of MDPI and/or the editor(s). MDPI and/or the editor(s) disclaim responsibility for any injury to people or property resulting from any ideas, methods, instructions or products referred to in the content.